# The Use of Inertial Altitude in the Determination of the Convective-Scale Pressure Field over Land

MARGARET A. LEMONE AND LESLEY F. TARLETON

*National Center for Atmospheric Research,* Boulder, Colorado 80307*

(Manuscript received 23 January 1986, in final form 9 May 1986)

ABSTRACT

Pressure perturbations are measured from an aircraft by subtracting its pressure altitude from its actual altitude. The pressure perturbation is equal to the resulting "D-value" multiplied by the acceleration of gravity and density of air. Normally, the actual altitude is measured using a radar altimeter; but this becomes increasingly difficult over increasingly complex terrain.

Here, we document a technique in which inertial altitude is used instead of radar altitude, eliminating the need for extremely accurate navigation or simple terrain, and apply it to document the pressure field at the base of an evolving cumulus congestus in CCOPE. Analysis of both this case study and aircraft self-calibration maneuvers in clear, undisturbed air suggests that a D-value (pressure) accuracy of 2 m (20 Pa) is achievable at cumulus–congestus scales. This accuracy is degraded, however, if the phenomenon of interest is large compared to the flight track.

## 1. Introduction

Pressure fields in hurricanes (see Gentry, 1964; Hawkins and Imbembo, 1976; Willoughby et al., 1982) and in highly baroclinic zones aloft (Shapiro and Kennedy, 1981), have been determined from aircraft flying over the ocean by taking the difference between the pressure altitude, determined from a standard or environmental atmosphere, and the actual altitude which has been determined by a high-precision radar altimeter (e.g., Brown et al., 1981). The pressure field is proportional to the "D-value" (radar altitude minus pressure altitude), via the hydrostatic equation.

In these works, the D-values were measured over water because of the difficulty in interpreting the radar altitude over irregular terrain—a one-meter variation in topography is equivalent to about a 10-Pa (0.1 mb) variation in pressure. However, Shapiro and Kennedy (1982) and Rodi and Parrish (personal communication, 1986) have succeeded in measuring D-values over land in their studies of jetstreams by combining accurate horizontal navigation with accurate representation of the topography. In Shapiro and Kennedy's study the mesosynoptic scale emphasis and the gently sloping terrain over West Texas made inertial navigation system (INS) positions less critical, and the occasional escarpment that showed up in the radar–altitude record enabled improvement in position. Rodi and Parrish (personal communication, 1986), focusing on smaller scales, have updated the INS positions with frequent DME (Distance-Measuring Equipment, used in aircraft navigation) updates to increase their position accuracy.

Here, we use inertially-stabilized vertical accelerometers to determine the actual altitude, to obtain the pressure field at the base of a cumulus congestus cloud. The technique is closely related to that used by Ramond (1978) to find the pressure field upwind of a convective cell, but with refinements that make it applicable to more turbulent regimes. Flight plans and instrumentation are discussed in section 2. Section 3 discusses the calculation of the D-value. In section 4 we use aircraft calibration maneuvers in clear air and a case study to evaluate the technique and explain some of the steps in the calculations. We conclude that the technique can produce D-values accurate to 2 m (0.2 mb or 20 Pa) for scales of at least 5–20 km, and that accuracy could be improved with better instrumentation, better flight planning, and correction for flow distortion around the sensor.

## 2. Instrumentation and data collection strategy

### *a. Instrumentation*

The pressure and altitude data used in this paper were collected at a 1-sec rate from the NCAR Queen Airs 304D and 306D, during the 1981 Cooperative Convective Precipitation Experiment (CCOPE; Knight, 1982). During CCOPE, the static pressure on both NCAR Queen Airs was measured with Rosemount 1201F variable-capacitance pressure transducers, attached by 275 cm of hosing (30 cm of 0.31 cm diameter hose; 245 cm of 0.63 cm diameter hose) to the static pressure ports of the Pitot-static tube (Fig. 1). Their specified accuracy is ±1 mb, assuming the transducer is exposed to $<1$ K min$^{-1}$ temperature change, with a relative (to mean pressure) accuracy on a straight-and-level flight leg of $\sim 1$ Pa based on the stated accuracies of true airspeed measurements (1 m s$^{-1}$) which are ob-

* The National Center for Atmospheric Research is sponsored by the National Science Foundation.

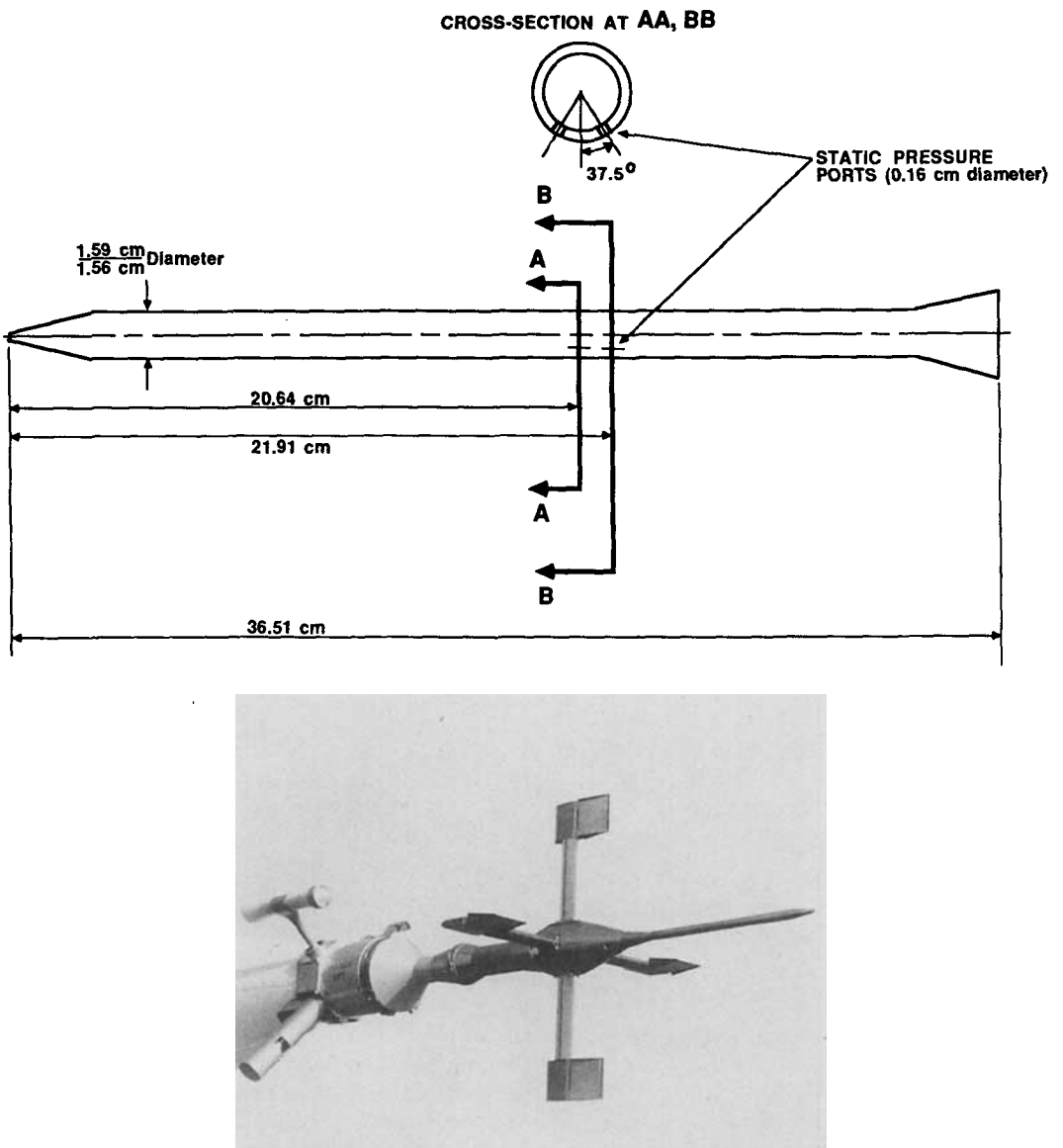


FIG. 1. (a) Drawing of the Queen Air pitot-static system used during CCOPE. The static ports are located on the sides of the pitot tube. (b) Picture of the Queen Air gust probe including the pitot-static system.

tained from similar instrumentation (Lenschow, 1972). The static pressures have been corrected by NCAR's Research Aircraft Facility to lessen the dynamic-pressure effects which result from the airstream impinging on the static ports. However, changes in the attitude angles of the airstream with respect to the aircraft remain a potential source of error, along with rapid altitude (temperature) changes, and the applied correction itself.

The altitudes of both aircraft are measured with inertial navigation systems (INS) which integrate the output of a set of inertially stabilized vertical accelerometers. Ground speed is measured by integrating the horizontal-accelerometer output. Accuracies are within kilometers and can be improved by renavigation (Fankhauser et al., 1985).

The performance of these data systems and their impact on the D-value calculation will be discussed below.

### *b. Data collection strategy*

The idealized flight patterns, which were designed to measure vertical mass and moisture flux a few hundred meters below cloud base, are pictured in Fig. 2. In pattern A-1 each Queen Air flew a racetrack pattern covering a slightly different area of the main up-

draft feeding a cumulonimbus cloud, but allowing for intercomparison of measurements along the portion of the pattern penetrating the center of the updraft. In pattern A-2, sometimes flown in combination with A-1, the aircraft flying the racetrack along the long axis of the updraft would radio the location of the updraft maximum to the second plane, which could then make a pass along the short axis of the updraft through the updraft maximum. Often, the "racetrack" pattern of A-1 or A-2 was flown with one aircraft instead of two.

Pattern A-3 was designed for smaller cumulus congestus or cumulus congestus just evolving into cumulonimbus, and usually involved only one aircraft. Here, transects were made 100–300 m below cloud base, along and normal to the long axis of the cloud which was assumed to align with the shear from cloud base to cloud top. The aircraft focused on the "hard," or sharply defined, cloud base, which generally corresponds to the cloud's main updraft (Marwitz et al., 1972).

After completion of the cloud-base maneuvers, the aircraft frequently did a series of calibration manuevers in which attitude, heading, and true air speed were varied. These were for the purpose of determining the in-flight characteristics of the aircraft sensors, and they proved useful in studying the response of static pressure sensors and the INS to aircraft maneuvers.

## 3. Evaluation of the D-value

The steps in estimating the D-value are summarized in the flow-chart in Fig. 3, which can be referred to in the course of this section, and section 4, in which error sources are discussed.

The D-value is given by the equation

$$D = \text{Inertial Altitude} - \text{Pressure Altitude} \quad (1)$$

and related to the pressure, via

$$p' = \rho D g \quad (2)$$

where $\rho$ is the air density, $g$ the acceleration of gravity, and $p'$ is the departure of the local pressure from that for the reference atmosphere (that used in calculating the pressure altitude).[1]

### a. Pressure altitude

The pressure altitude is found from integrating the hydrostatic equation, under the assumption of a constant lapse rate $\Gamma_d$ in the virtual temperature, defined such that a decrease in temperature with height is positive:

$$z - z_0 = \frac{T_{v_0}}{\Gamma_d}\left[1 - \left(\frac{p}{p_0}\right)^{\Gamma_d R/g}\right] \quad (3)$$

where $R$ is the gas constant for dry air (287 $K^{-1}$ $m^2$ $s^{-2}$) and $p_0$ and $T_{v_0}$ are the pressure and virtual temperature at some reference height $z_0$. Here the reference altitude and pressure, $z_0$ and $p_0$, are the average altitude and pressure of the aircraft, and $T_{v_0}$ and $\Gamma_d$, the virtual temperature and lapse rate at the reference altitude, are found from an environmental sounding. The acquired altitude is then interpolated and advanced 0.3 sec to allow for the time lag of the pressure sensor (see section 4).

### b. Calculation of inertial altitude—standard calculations

The aircraft vertical velocity $w_p$ is found from integrating the inertial acceleration, after correcting for the vertical component of the Coriolis force, centrifugal force, and the variation of gravity (Lenschow, 1972), via

$$w_{p_t} = w_{p_{t-\Delta t}} + \Delta t(a + g_{\text{corr}} + a_{\text{corr}}) \quad (4)$$

where $\Delta t$ is the time between measurements (here, 1 sec), $a$ is the uncorrected acceleration at $t - \Delta t/2$, and the two correction terms are evaluated for time $t$. The slight mismatch in time creates negligible error since both $a_{\text{corr}}$ and $g_{\text{corr}}$ are fairly slowly changing functions. The gravitational correction $g_{\text{corr}}$ is given by

$$g_{\text{corr}} = 9.7959 - 9.780356(1.0 - 0.31391116 \times 10^{-6}\,\text{PALT}) \times (1 + 0.0052885\,\sin^2(\text{lat})),$$

where PALT is the pressure altitude and "lat" represents latitude (Kayton and Fried, 1969). The correction $a_{\text{corr}}$ accounts for Coriolis and centrifugal accelerations, and is given by

$$a_{\text{corr}} = 2\Omega U \cos(\text{lat}) + \frac{U^2 + V^2}{R}.$$

Here, $U$ is the aircraft east–west ground speed, $V$ is the north–south ground speed, $R$ is the height of the aircraft above the center of the earth, and $\Omega$ is the angular velocity of the earth.

### c. Calculation of the inertial altitude—Nonstandard corrections

Even after these corrections, the aircraft vertical acceleration consistently shows a constant offset, presumably due to a bias in the INS vertical accelerometers. This offset results in an aircraft vertical velocity that varies linearly with time, and an inertial altitude that varies quadratically. The constant bias is removed for all flights by determining the slope of the vertical

[1] It is perhaps more logical to calculate $p$ from the difference between the measured pressure and the pressure from the inertial altitude and an environmental sounding. This more direct technique also eliminates the misleading impression that (2) gives only the hydrostatic pressure perturbation. However, we use D-values for historical reasons and note that it can easily be shown that the perturbation pressure, $p'$, in (2) is from dynamic as well as hydrostatic sources. This is done to good approximation by using (3) to compare $p'$ from (2) to the $p'$ obtained directly as described here.

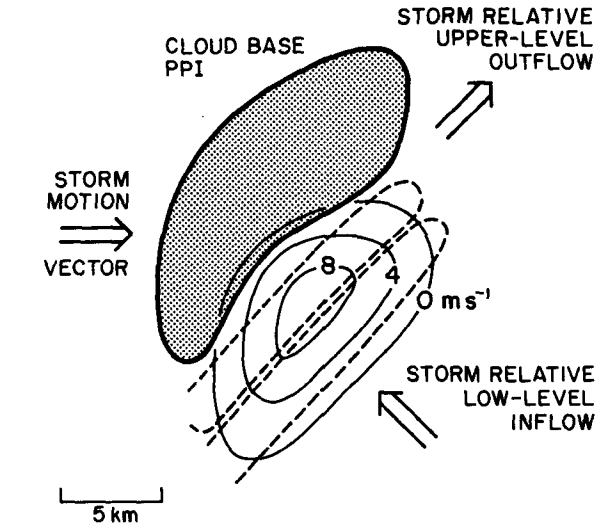


PATTERN A-1

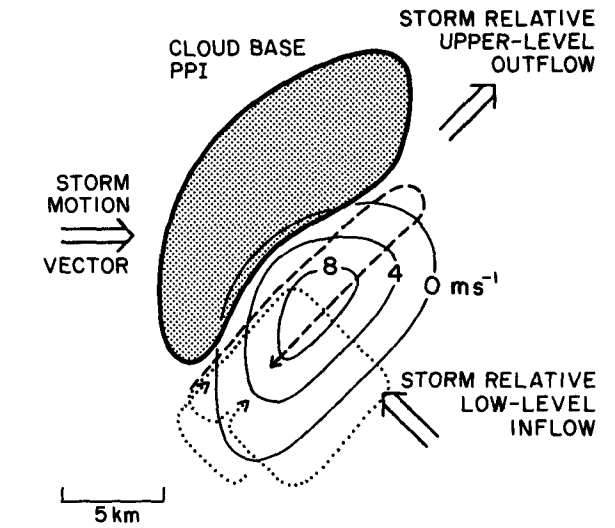


PATTERN A-2

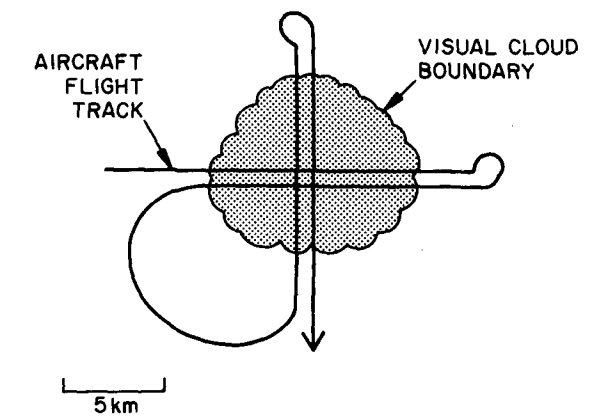


PATTERN A-3

velocity line for the entire flight, and using the result to linearly detrend the aircraft velocity, leg by leg, before integrating to determine inertial altitude.

The integration in (4) to determine the aircraft vertical velocity is done with the assumption that $w_p = 0$ at the beginning of the leg. The resulting vertical velocity is then corrected linearly, assuming that the measured change in aircraft inertial altitude is equal to the measured change in pressure altitude. This is equivalent to assuming that the D-values at the leg end points are equal. The vertical velocity is then integrated to obtain the inertial altitude, under the assumption that the initial inertial altitude is equal to the initial pressure altitude, equivalent to assuming $D = 0$, or that the flight legs begin in an undisturbed environment. Thus, we assume that $D = 0$ at both ends of the flight legs. The D-value can now be computed from (1).

Unfortunately the D-value thus obtained still shows quadratic variation due primarily to a bias in the vertical accelerometer. Assuming (a) that the D-value error is entirely due to the INS vertical acceleration error, and (b) that the acceleration error is constant during a leg, we can correct for it by removing some sort of "best-fit" quadratic. The two techniques used are the "equal area method" and the least-squares fit, discussed below. In both techniques we again apply the assumption that the D-values are zero at the ends of the leg.

In the equal area method the subtracted quadratic has the form

$$D_{\text{error}} = c(t^2 - t_f t) \tag{5}$$

where $c$ is a constant, $t$ is time, and $t_f$ is the last time of the flight leg (the first time being set to zero). The constant $c$ satisfies

$$\sum_{i=1}^{n} D_{ui} - c \sum_{i=1}^{n} (t_i^2 - t_i t_f) = \sum_{i=1}^{n} D_{ci} = 0 \tag{6}$$

where $D_c$ and $D_u$ are the corrected and uncorrected D-values and there are $n$ evenly-spaced data points. That is, the area of the positive and negative corrected $D$-excursions sums to zero.

Since (5) and (6) put such severe constraints on the D-value, an alternative was tried, removing a least-squares best-fit quadratic from $D$ (again under the condition that $D = 0$ at $t = 0$) and then removing the linear trend from the "corrected" D-value so that $D = 0$ at both ends of the flight leg.

The best-fit quadratic is of the form

$$y = a_1 t + a_2 t^2 \tag{7}$$

where $t$ is time, $a_1$ is given by

$$a_1 = \frac{\sum t_i^4 \sum D_{ui} t_i - \sum t_i^3 \sum t_i^2 D_{ui}}{\sum t_i^2 \sum t_i^4 - \sum t_i^3 \sum t_i^3}$$

FIG. 2. Flight patterns flown by the Queen Airs at the base of cumulonimbus (A-1, A-2) and cumulus congestus (A-3) clouds during CCOPE. A-1 was often flown with just one aircraft.

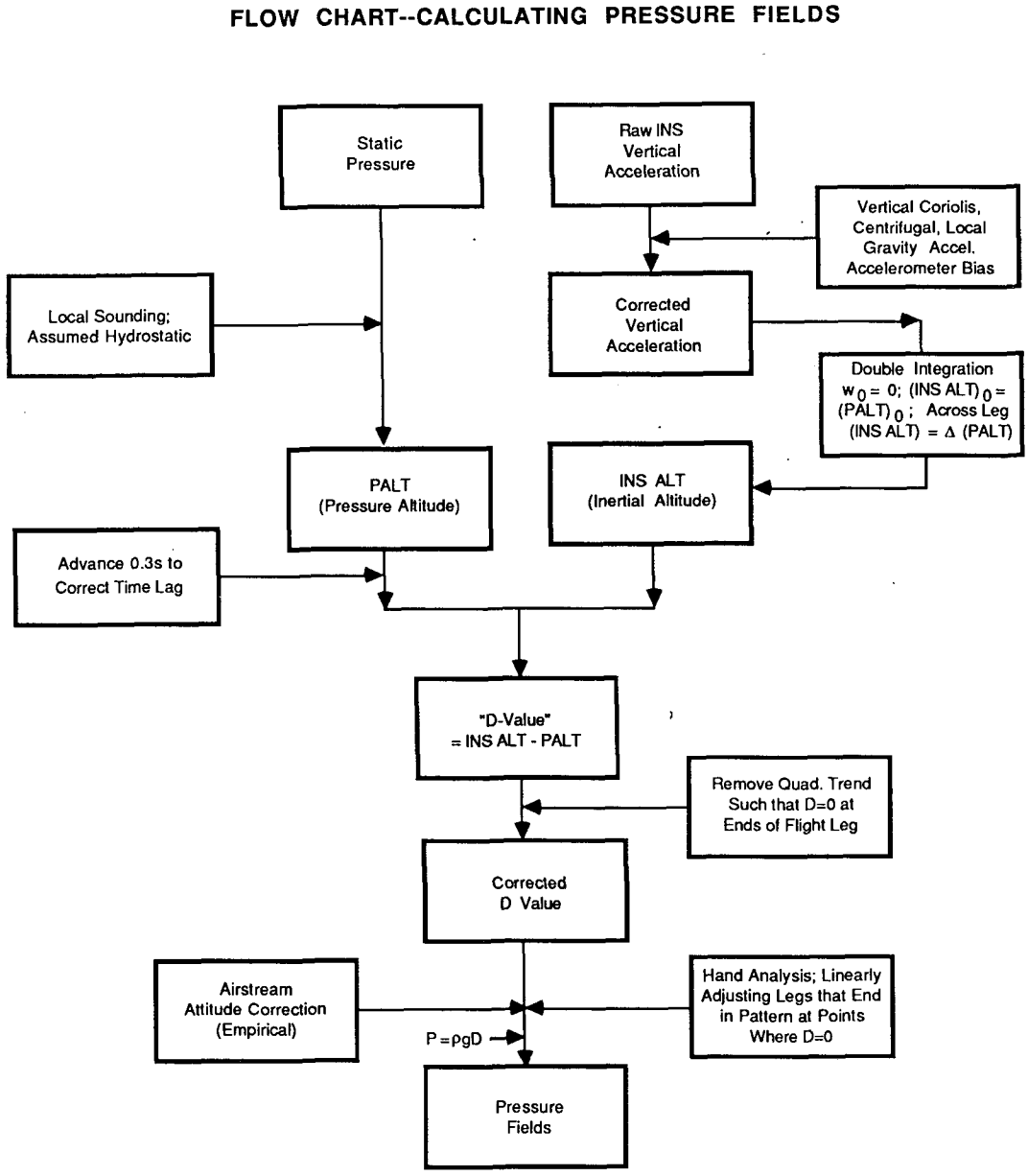


FIG. 3. Flow-chart of the D-value computation.

and $a_2$ by

$$a_2 = \frac{\sum t_i^2 D_{ui} \sum t_i^2 - \sum t_i D_{ui} \sum t_i^3}{\sum t_i^2 \sum t_i^4 - \sum t_i^3 \sum t_i^3}$$

where the summations are for all the points in the flight leg.

Clearly neither detrending technique is optimum. Both use the entire flight leg to determine the accelerometer error, a poor technique if much of the D-value variation represents real pressure change. Furthermore, both put constraints on the relationship between high and low pressure regions, and finally, they force the D-value to be zero at the end points of the leg. However, we believe that the two techniques are the best possible under the circumstances. Using just the "environment" outside the cloud to determine the best-fit quadratic was considered and discarded for two reasons. First, the aircraft generally turned very soon after completion of the updraft penetration so that there wasn't much environment sampled, and second, the temperature, humidity, and wind measurements showed the environment to be strongly interacting with the cloud. Fortunately, the two techniques produced qualitatively similar results, with the "equal-area" technique better suited to the updrafts/clouds large

compared to the length of the flight track, and the quadratic least-squares fit line better suited to clouds small compared to the length of the flight track.

*d. Analysis of the pressure fields*

The resulting D-values are plotted on flight tracks in storm-relative coordinates that were produced by computer software developed for the analysis of aircraft data collected in CCOPE (Fankhauser et al., 1985). When a flight track ends inside the borders of the pattern defined by longer tracks, the end point D-value is set to the value determined by analysis of the longer flight track data. The corrections of the remainder of the leg are linearly interpolated between the endpoint corrections.

## 4. Evaluation of the technique

The pressure measurement technique has been evaluated in two ways. First, D-values were calculated during aircraft calibration maneuvers in clear, undisturbed air, where $D$ should be zero. Second, we evaluated $D$ fields near the base of several clouds. In the latter case, the fields could be judged on the basis of repeatability and comparison with models. Both techniques suggest an accuracy, *on the convective scales,* of the order 1–2 m.

*a. Aircraft calibration maneuvers*

Aircraft calibration maneuvers have been useful in discovering problems with aircraft sensors and corrections needed for the data, and in estimating the accuracy of the D-values obtained. During the maneuvers, for consecutive periods of two to three minutes, the pilots varied the pitch angle, side-slip angle, and true air speed; and then flew 2–3 min legs at opposite headings. If possible, both Queen Airs did a complete set of maneuvers on each flight, in clear, undisturbed air.

1) PITCH MANEUVERS

Here the aircraft varies in altitude sinusoidally, with periods (in the runs analyzed) from 9 to 26 sec and amplitudes from 12 to 41 m. An example appears in Fig. 4. Based on these maneuvers, the boom pressure was found preferable to the fuselage pressure, and the local environmental sounding replaced the NACA standard atmosphere in the pressure–altitude calculations.

The pitch maneuvers revealed a 0.3 sec time lag of the pressure measurements with respect to the inertial altitude. From (1), for sinusoidally-varying inertial and pressure altitudes of amplitude $A$ and a pressure altitude phase lag of $\phi$

$$D = \text{inertial altitude} - \text{pressure altitude}$$

$$D = A[\sin\omega t - \sin(\omega t - \phi)],$$

$$D \approx A \sin\phi \cos\omega t \qquad (8)$$

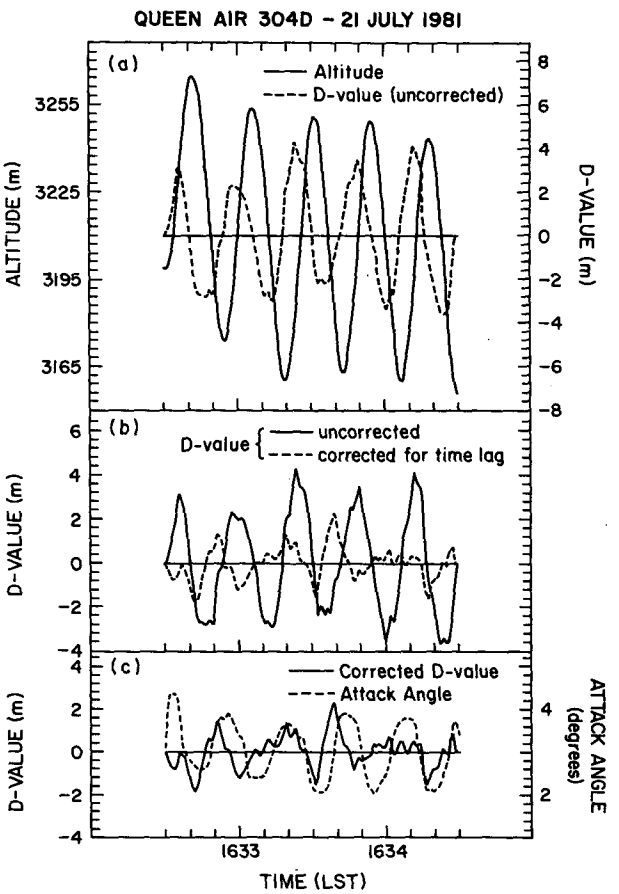


FIG. 4. Response of D-value error to pitch maneuvers in clear, undisturbed air ($D = 0$). (a) altitude, solid line, D-value before time-lag correction, dashed line; (b) D-value before time lag correction (solid line) compared to D-value after time lag correction (dashed line); (c) D-value corrected for time lag (solid line), attack angle (dashed line). Horizontal lines denote leg average.

since, from examination of the time series, we know that $\phi$ is small. The phase relationship between $D$ and altitude is consistent with what is observed in the pitch maneuvers (e.g., Fig. 4a). By substituting $D$ and $\omega$ into (8) for several pitch maneuvers, we found the phase lag $\phi$ corresponds to a time lag of 0.3 sec $\pm$ ~0.025 sec for both aircraft, consistent with the results of cross-spectral analysis. Removal of this phase lag reduces the amplitude of the spurious D-values by about a factor of 2 (Fig. 4b). This empirically-determined pressure time lag was used rather than a modeled one (see, e.g., Iberoll, 1950) because of the complexities introduced into the calculation by the change in diameter of the tubing from the static ports to the pressure transducer.

Much of the remaining spurious D-value signal in Fig. 4c is due to angle-of-attack and true airspeed variation. Since some of the remaining error is undoubtedly also due to imperfections in accounting for altitude changes and time lag, the attack angle and true airspeed contributions to D-value error will be evaluated using the true-airspeed variation maneuvers.

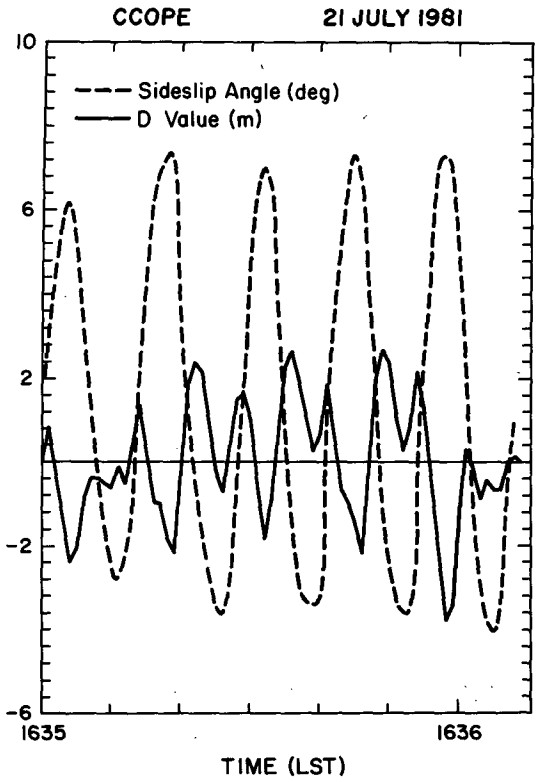


FIG. 5. As in Fig. 4 but for response of D-value error to sideslip maneuvers. D-value (solid line); sideslip angle (dashed line).

### 2) SIDESLIP MANEUVERS

Figure 5 shows the response of the D-values to sideslip changes. Minima in D-value are correlated with extrema in sideslip. Thus (1) implies that maxima in pressure altitude (minima in pressure) are associated with maximum sideslip deviation. The near-symmetry of the response (The difference in D-value is related to the size of the sideslip rather than its sign.) reflects the symmetric arrangement of the static ports in Fig. 1. The illustrated response is typical, with a 4.5° oscillation in sideslip angle giving about a 2-m spurious D-value oscillation.

### 3) TRUE AIRSPEED VARIATIONS

Figure 6a shows the D-value, true airspeed, and angle of attack for a roughly sinusoidal variation of true airspeed. The angle of attack maxima are associated with minima in $D$ (or minima in static pressure) and conversely. (Negative angles of attack were not observed.) An analogous relationship of angle of attack, true airspeed, and static pressure is evident in the Queen Air tower fly-by data of Biter (personal communication, 1983) which shows increased static pressure at higher true airspeeds (smaller angles of attack).

In Fig. 6, the D-value oscillation associated with true airspeed variation is slightly larger than average. More typically a variation of true airspeed from 60 to 90 m $s^{-1}$ ($\sim 1°-6°$ in angle of attack) is associated with a 1–2 m variation in $D$.

### 4) REVERSE-HEADING MANEUVERS

These consisted of two short straight-and-level legs separated by a 180° turn at a rate of 2–3° $s^{-1}$. During the turns the D-values are offset by $\geq \pm 2$ m, reaching as high as ±6 m on the fastest turns. This is related primarily to deviations in the angles between the airflow and the fuselage.

These turns are excluded from the data analysis and particular care is taken in selecting leg end points, since setting a spurious D-value to zero can alter the D-values for the entire leg.

## *b. Analysis of a real case: The cumulus congestus cloud of 21 July 1981*

This particular case, which is from the 1981 CCOPE experiment, is presented to illustrate the analysis technique and its strengths and weaknesses. On 21 July,

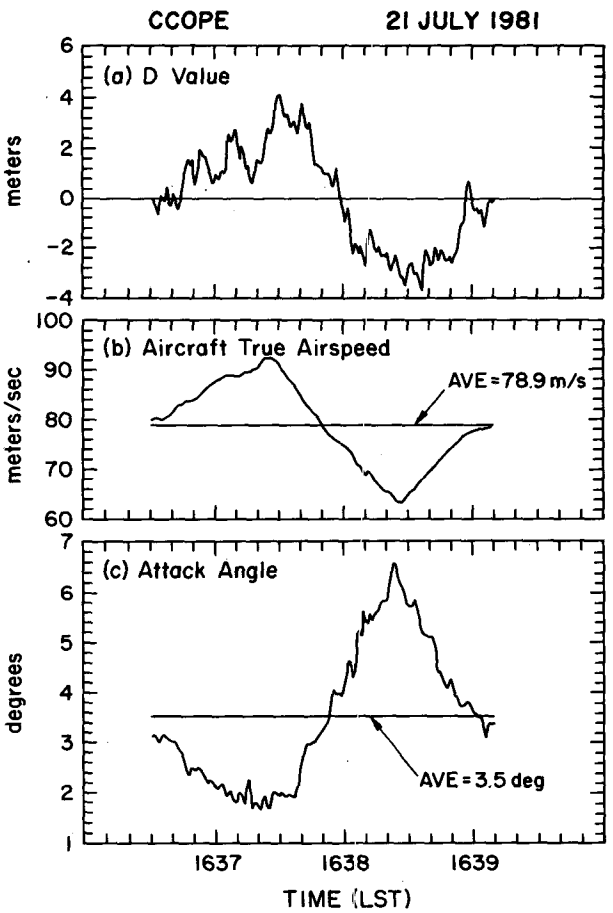


FIG. 6. As in Fig. 4 but for response of D-value error to true airspeed variation. (a) D-value; (b) true airspeed; (c) attack angle.

the NCAR Queen Air 304D flew cross patterns relative to the cloud (patterns A-3 in Fig. 2) and then across-updraft legs ("racetracks," as in patterns A-1 or A-2) through the updraft at the base of a growing cumulus congestus. During the hour the aircraft penetrated the updraft, the cloud began precipitating and split into two cells, only the southern of which persisted, and then began to rapidly weaken. The supporting data have been generously supplied by G. Barnes, (personal communication, 1985) who is documenting the life history of the cloud in a forthcoming publication.

A typical time series of D-values, found using the procedure described above, appears in Fig. 7. The vertical velocity is also presented in the figure. The high-frequency oscillations from the pressure measurement, [pressure altitude in (1)], are filtered out by eye before plotting on the flight tracks. No objective filtering is done since the legs are short and the D-values are compromised in turns, so that spurious values would be communicated to much of the good data through a filtering procedure, particularly for large numbers of weights.

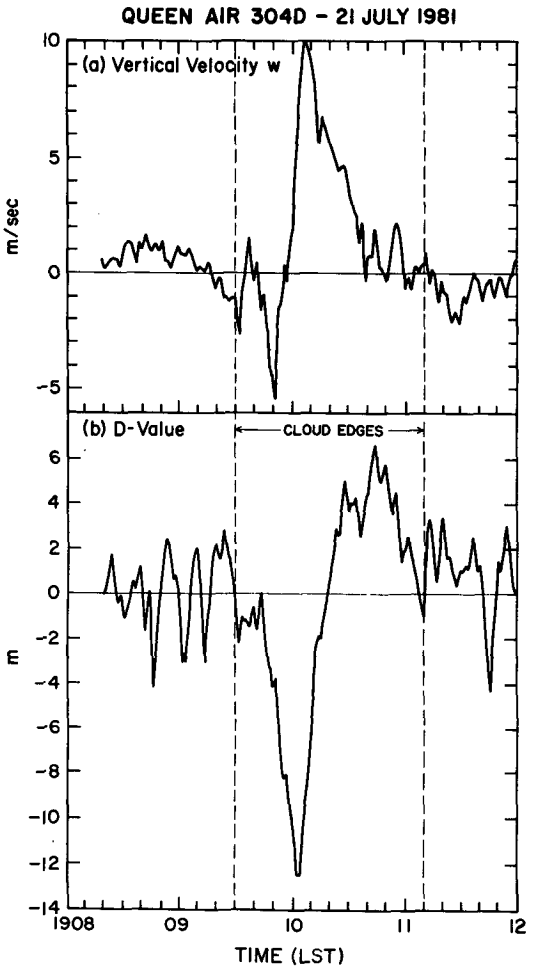


FIG. 7. (a) Vertical velocity and (b) D-value for the NCAR Queen Air 304D flying a straight-and-level leg a few hundred meters below cloud base, through the updraft feeding the cloud, on 21 July 1981. Vertical dashed lines denote cloud edges.

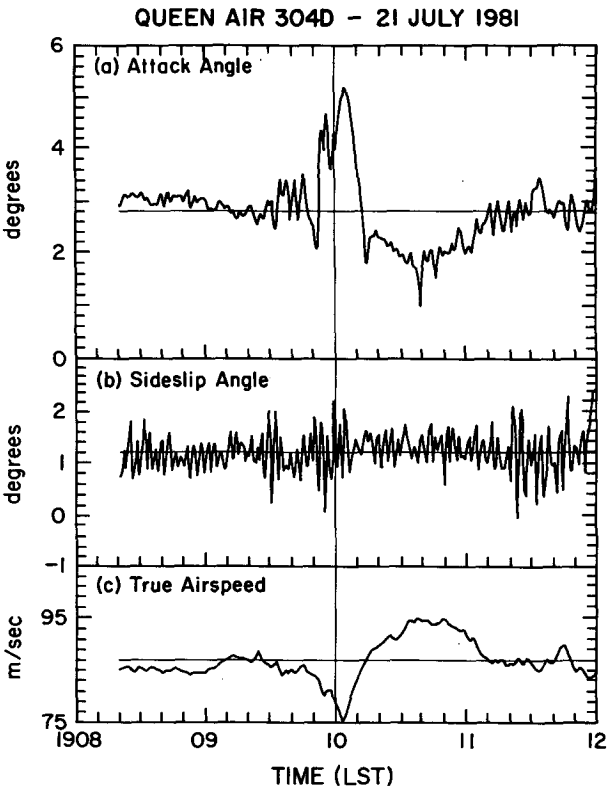


FIG. 8. As in Fig. 7 but for (a) angle of attack; (b) sideslip; and (c) true airspeed. Horizontal lines denote leg average.

The angle of attack, sideslip, and true airspeed are presented for the same times in Fig. 8. Note from the figures that the angle of attack and true airspeed vary the most around the interesting D-value feature. Since they vary in the same sense as in the true airspeed variation maneuvers (Fig. 6a), the angle-of-attack is used in a rough correction procedure. Analysis of the true-airspeed variation maneuvers in CCOPE suggests a D-value error (correction) of $-(+)0.77\alpha'$, where $\alpha'$ is the attack-angle departure from the leg mean.[2] The largest correction applied in this case was less than 3 m in the D-value extrema. (It did not seem wise to use the pitch maneuvers since other corrections had been applied before obtaining the D-value.)

Before the plotting of the D-value field, the flight legs (Table 1) were plotted in a coordinate system moving with the cloud using the procedure outlined

[2] This correction applies to the Queen Airs in CCOPE only and must be determined independently for different aircraft in different experiments.

TABLE 1. Flight legs used in analysis of the 21 July cloud.

| Leg | Time (MDT) |
|---|---|
| 1 | 1835:35 – 1839:15 |
| 2 | 1841:34 – 1844:10 |
| 3 | 1845:40 – 1848:42 |
| 4 | 1850:20 – 1854:20 |
| 5 | 1855:50 – 1859:05 |
| 6 | 1904:20 – 1907:00 |
| 7 | 1908:20 – 1912:00 |
| 8 | 1913:40 – 1918:37 |
| 9 | 1920:20 – 1924:30 |
| 10 | 1926:20 – 1931:16 |

in Fankhauser et al., 1985. The cloud speed, found by tracking radar echoes and updraft positions, was from the west (289°) at 15.5 m $s^{-1}$ (Barnes, personal communication, 1985).

The D-value field is plotted for data centered about five selected times in Fig. 9 with the corresponding vertical velocity field in Fig. 10. From Table 1 and the figures, each frame represents data from three or four flight legs. The distance markings, standard for CCOPE, denote kilometers to the north and east of the CP-2 radar. The times are spaced at 11–14 min intervals, except for the first two patterns, whose data overlap except for legs 1 and 5 in the table. We note that the general features of the D-value field are preserved for the first two times, with a band of low pressure running roughly north–south, flanked by high pressure to the east and west. The differences are due to the addition and subtraction of flight legs as well as evolution. The cross leg from 1836 to 1839 provides more detail to the pressure analysis centered around 1848, while the 1856–1859 flight leg extends the low pressure area westward. Similar behavior exists in the vertical velocity field, with a western and eastern updraft. The notable contrast is the appearance of a strong upward vertical velocity maximum at the cloud's southwestern edge at the northern part of the low pressure area.

Better time continuity in both vertical velocity and pressure features is achieved once the aircraft focuses on the major updraft–downdraft couplet (lower three frames). Although details change, the vertical velocity extrema correspond to the greatest horizontal changes in pressure. The close to 90° phase differences between pressure and vertical velocity is observed in all cases thus far examined. A similar relationship is evident for plume scale motions in Wilczak and Businger's work, if one compares Fig. 2b of Wilczak (1984) to Fig. 6 of Wilczak and Businger (1984).

The 90° phase lag is predicted in a linearized form of the momentum equation in Rotunno and Klemp (1982). Figure 14 of Rotunno and Klemp (1985) shows the vertical gradient of pressure roughly 90° out of phase with the updraft in the numerical simulation of a severe thunderstorm. In the figure, we see the updraft growing on its southern side due to upward acceleration associated with the vertical pressure gradient.

Although the presence of the downdraft complicates the picture, the direction of propagation of the 21 July cloud is correctly predicted by the pressure field, if we assume that the pressure perturbation decreases nearer the surface. Under these conditions, the air should be accelerated upward on the southern side of the updraft, and the updraft should be decelerated on the northern side, suggesting southward propagation. Indeed the cloud does travel southward relative to the mean flow through its depth.

Repeatability and physical reasonableness lend credence to the technique, but do not give a feel for its accuracy. However, in each pattern there are a number of places traversed by the aircraft more than once, in addition to the repeated pressure extrema. Comparison of both the points of intersection and the pressure extrema yields differences in $D$ typically less than 2 m.

## 5. Conclusions

Aircraft can be used to measure the perturbation pressure fields (D-values) on the cumulus–congestus scale by comparing the pressure altitude to the inertial altitude. Aircraft calibration maneuvers, which isolate the effects of both aircraft acceleration and airflow relative to the aircraft, and case studies, where an evolving field is measured repeatedly, both indicate that D-values can be measured to within about 2 m on this scale. The accuracy is degraded if the scale of the phenomenon of interest is large compared to the flight track or if the flight track is not flown properly.

The D-value is equal to the difference between the real (here, inertial) and pressure altitudes. Great care is required in computing both. Pressure altitudes are calculated assuming hydrostatic balance in the environmental sounding. A rough "removal" of airflow effects around the static ports by using an angle-of-attack D-value error relationship improves results slightly. Inertial altitudes require the use of the standard Coriolis, centrifugal force, and gravity corrections, plus the removal of the bias in the vertical accelerometer, accomplished here by quadratic detrending under the assumption that the pressure and inertial altitude are equal at the end points of the flight leg (tantamount to assuming no pressure perturbation in the "environment"). Time lags between the pressure sensor and inertial navigation system should be accounted for before computation of the D-value.

The efficacy of the technique is limited by the flight pattern and the time and space scales of the phenomenon observed. The D-values are often compromised in turns. If flight legs are too short compared to the observed field, the quadratic detrending can severely distort the signal, and the assumption that $D = 0$ at the ends of the flight legs is violated. If flight legs are

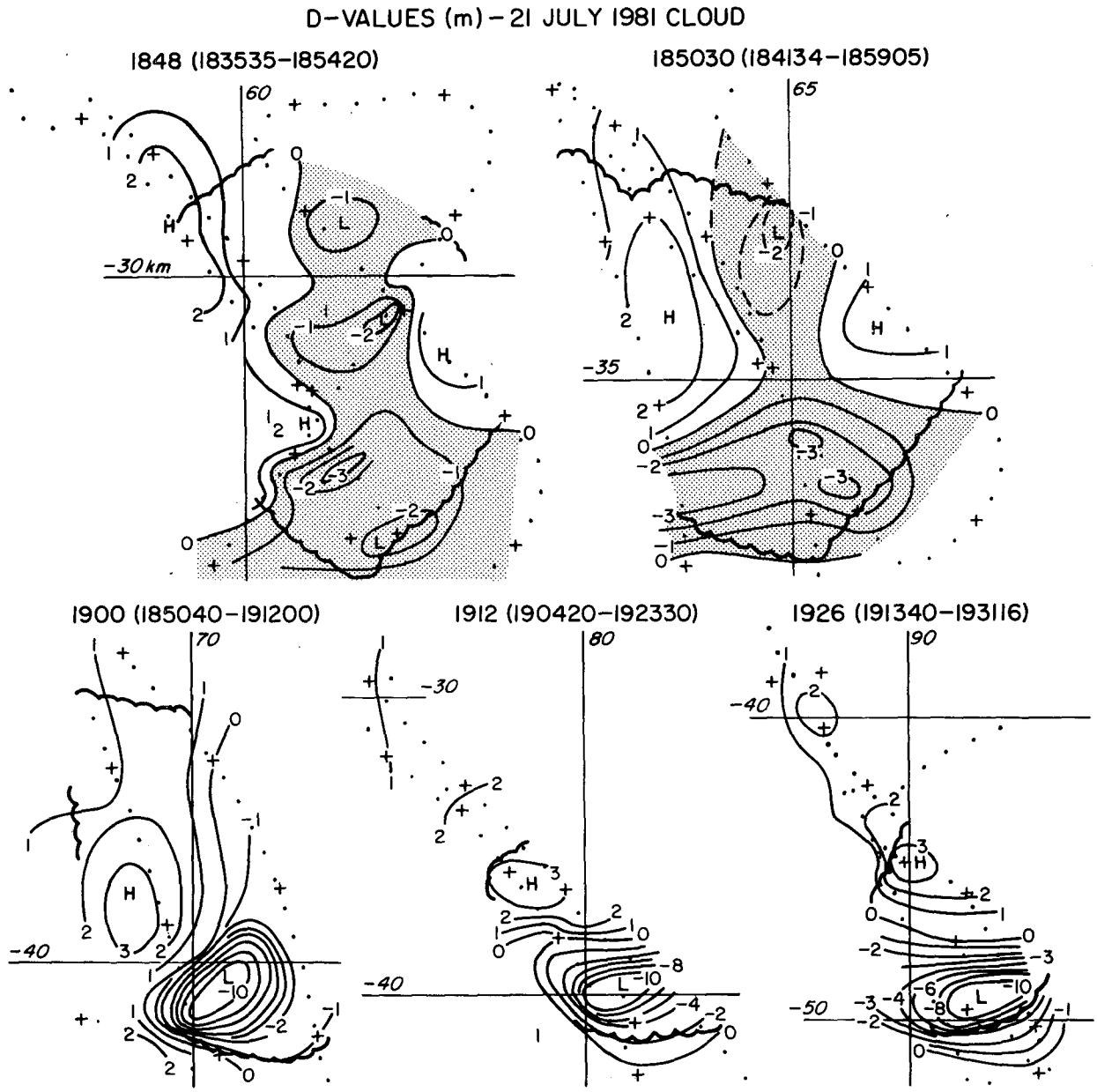


FIG. 9. The D-value field for selected times (MDT), at the base of the cumulus congestus of 21 July 1981. The flight tracks are plotted with dots at 12-sec intervals and crosses which mark the even minutes. Scallops denote approximate location of cloud edge. To convert to Pascals, multiply by 7.9; to millibars, by 0.079.

longer than ~10 minutes, the inertial altitude is less reliable. Finally, the observed field can change during the flight pattern.

Better accuracies are possible with better pressure sensors, better inertial navigation systems, and better corrections for the effects of airflow around the static ports. Improved response would be achieved with shorter tubing of constant diameter between the static ports and the sensor. Recording pressure at a faster rate would eliminate the necessity of interpolating to correct for the time lag between the two altitude-measuring systems. Better inertial navigation systems would provide more stable estimates of altitude at lower frequencies. The pressure field could be computed over a broad range of frequencies by combining the technique discussed in this paper (at high frequencies) with

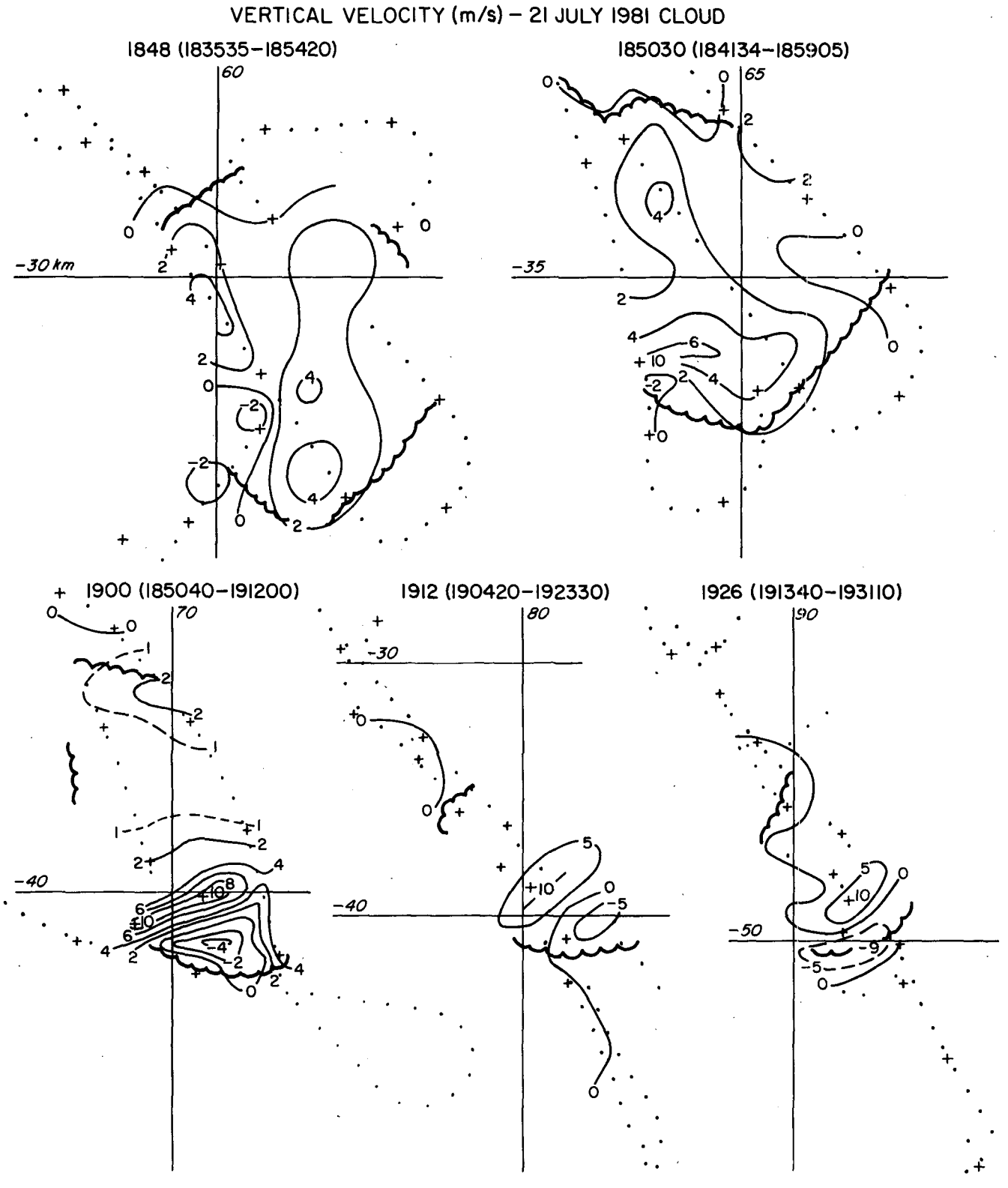


FIG. 10. As in Fig. 9 but for vertical velocity.

the technique of Rodi and Parrish (at low frequencies), which obtains actual altitude from accurate horizontal navigation and a radar altimeter.

*Acknowledgments.* The authors wish to acknowledge those who designed the Queen Air cloud-base updraft flight patterns, and the crews who executed them with such precision. James C. Fankhauser, Gary M. Barnes, Carlos Latorre, and Charles A. Knight provided us with flight tracks and supporting data for analysis of pressure measurements on several days in CCOPE. Robin Vaughan's help in reading the aircraft tapes was invaluable. Cleon Biter and Don Lenschow provided guidance in the subtleties of correcting inertial navigation system data, and Paul Spyers-Duran, Peter Hildebrand, and Richard Friesen provided valuable information on the Queen Air instrumentation. Finally, we wish to thank Sudie Kelly for prompt and accurate typing of the manuscript (especially the equations).

## REFERENCES

Brown, E. N., M. A. Shapiro, P. J. Kennedy and C. A. Friehe, 1981: The application of airborne radar altimetry to measurement of height and slope of isobaric surfaces. *J. Appl. Meteor.*, **20,** 1070–1075.

Fankhauser, J. C., C. J. Biter, C. G. Mohr and R. L. Vaughan, 1985: Objective analysis of constant-altitude aircraft measurements. *J. Atmos. Oceanic Technol.*, **2,** 157–170.

Gentry, R. C., 1964: A study of hurricane rainbands. National Hurricane Research Project Rep. No. 69, Hurricane Research Division, 85 pp. [NTIS PB 16841F].

Hawkins, H. F., and S. M. Imbembo, 1976: The structure of a small, intense hurricane—Inez 1966. *Mon. Wea. Rev.*, **104,** 418–442.

Iberoll, A. S., 1950: Attenuation of oscillatory pressures in instrument lines. *J. Res. Natl. Bur. Stand.*, **45,** 85–108.

Kayton, M., and W. R. Fried, 1969: *Avionics Navigation Systems.* Wiley & Sons, 666 pp.

Knight, C. A., 1982: The Cooperative Convective Precipitation Experiment (CCOPE), 18 May–7 August 1981. *Bull. Amer. Meteor. Soc.*, **63,** 386–398.

Marwitz, J. D., A. H. Auer, Jr. and D. L. Veal, 1972: Locating the organized updraft on severe thunderstorms. *J. Appl. Meteor.*, **11,** 236–238.

Ramond, D., 1978: Pressure perturbations in deep convection: An experimental study. *J. Atmos. Sci.*, **35,** 1704–1711.

Rotunno, R., and J. B. Klemp, 1982: The influence of the shear-induced pressure gradient on thunderstorm motion. *Mon. Wea. Rev.*, **110,** 136–151.

——, and ——, 1985: On the rotation and propagation of simulated supercell thunderstorms. *J. Atmos. Sci.*, **42,** 271–292.

Shapiro, M. A., and P. J. Kennedy, 1981: Research aircraft measurements of jet stream geostrophic and ageostrophic winds. *J. Atmos. Sci.*, **38,** 2642–2652.

——, and ——, 1982: Airborne radar altimeter measurements of geostrophic and ageostrophic winds over irregular topography. *J. Appl. Meteor.*, **21,** 1739–1746.

Wilczak, J. M., 1984: Large-scale eddies in the unstably stratified atmospheric surface layer. Part I: Velocity and temperature structure. *J. Atmos. Sci.*, **41,** 3537–3550.

——, and J. A. Businger, 1984: Large-scale eddies in the unstably stratified atmospheric surface layer. Part II: Turbulent pressure fluctuation and the budgets of heat flux, stress, and turbulent kinetic energy. *J. Atmos. Sci.*, **41,** 3551–3567.

Willoughby, H. E., J. A. Clos and M. G. Shoreibah, 1982: Concentric eyewalls, secondary wind maxima, and the evolution of the hurricane vortex. *J. Atmos. Sci.*, **39,** 395–411.